*INEEL/CON-99-00151*
*PREPRINT*

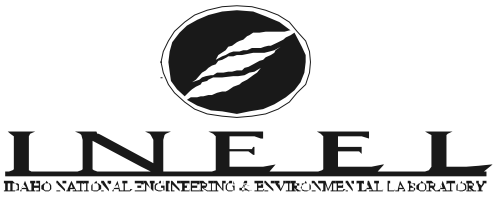


# A Model for Molten Fuel-Coolant Interaction During Melt Slumping in a Nuclear Reactor

**M. S. Sohal**
**L. J. Siefken**

**October 5, 1999 – October 8, 1999**

**9th International Meeting on Nuclear Reactor Thermal Hydraulics**



LOCKHEED MARTIN

Ninth International Topical Meeting on Nuclear Reactor Thermal Hydraulics (NURETH-9)
San Francisco, California, October 3-8, 1999.

# A MODEL FOR MOLTEN FUEL-COOLANT INTERACTION DURING MELT SLUMPING IN A NUCLEAR REACTOR

**M. S. Sohal and L. J. Siefken**

Idaho National Engineering and Environmental Laboratory
Idaho Falls, ID 83415-3815
sohalms@inel.gov, ljs@inel.gov

## KEY WORDS

Fuel-coolant interaction, model.

## ABSTRACT

This paper describes a simple fuel melt slumping model to replace the current parametric model in SCDAP/RELAP5. Specifically, a fuel-coolant interaction (FCI) model is developed to analyze the slumping molten fuel, molten fuel breakup, heat transfer to coolant, relocation of the molten droplets, size of the partially solidified particles that settle to the bottom of the lower plenum, and melt-plenum interaction, if any. Considering our objectives, the molten fuel jet breakup model, and fuel droplets Lagrangian model as included in a code TEXAS-V with Eulerian thermal hydraulics for water and steam from SCDAP/RELAP5 were used. The model was assessed with experimental data from MAGICO-2000 tests performed at University of California at Santa Barbara, and FARO Test L-08 performed at Joint Research Center, Ispra, Italy. The comparison was found satisfactory.

## 1. INTRODUCTION

The SCDAP/RELAP5 computer code (Allison, et al., 1996) is being developed at the Idaho National Engineering and Environmental Laboratory (INEEL) under the primary sponsorship of the U. S. Nuclear Regulatory Commission (NRC). It describes the overall nuclear reactor coolant system thermal hydraulic response, core damage progression, and, in combination with a code VICTORIA, fission product release and transport during severe accidents. This paper discusses a fuel-coolant interaction (FCI) model and its implementation in SCDAP/RELAP5.

### 1.1 Objective

Figure 1 shows a schematic view of the molten material from the reactor core slumping under gravity as a jet through the openings in the lower plenum structure and interacting with the coolant in the lower plenum. A simple fuel melt slumping model to meet the needs of the

SCDAP/RELAP5 code was developed to analyze the slumping molten fuel, molten fuel breakup, fragmentation, heat transfer to coolant and steam, relocation of the molten droplets, size of the partially solidified particles that settle to the bottom of the lower plenum, and melt-plenum interaction, if any.

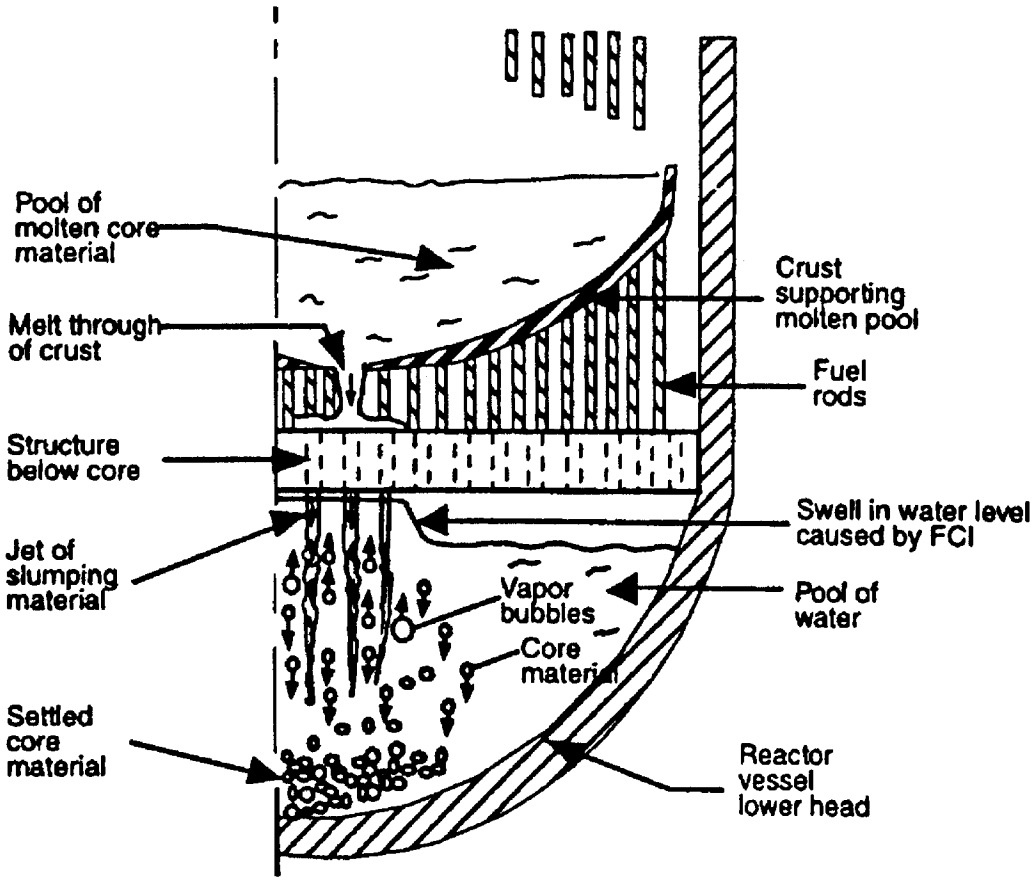


**Figure 1.** Schematic of molten material slumping into the lower plenum.

## 1.2 Background Literature

In a nuclear reactor, if normal and emergency coolant flows fail, the fission product decay heat would melt the fuel ($UO_2/ZrO_2$). The molten fuel flows through available openings in the plates and structure, and falls into the coolant contained in the lower plenum. The size and velocity of the molten fuel jet depend on its interaction with the plate structure encountered during its downward flow under gravity. Corradini et al. (1988, 1991) reviewed the phenomenon of molten fuel-coolant interaction, which under certain conditions may result in energetic steam explosion. When hot molten liquid contacts cold liquid, there is rapid energy transfer from hot liquid (fuel) to more volatile colder liquid (coolant). The coolant vaporizes and forms a film of steam around the liquid fuel (Figure 2b-c). For a period ranging from a few milliseconds to a few

seconds, the system is in a metastable state with a rise in local pressure. Whenever the vapor film destabilizes, fuel fragmentation takes place. This increases fuel surface area, which results in more vapor formation. The high pressure coolant vapor expands against the inertial resistance of the surroundings. Presently, we are concerned only with the nonenergetic FCI phenomena including molten fuel break-up, fragmentation, and mixing.

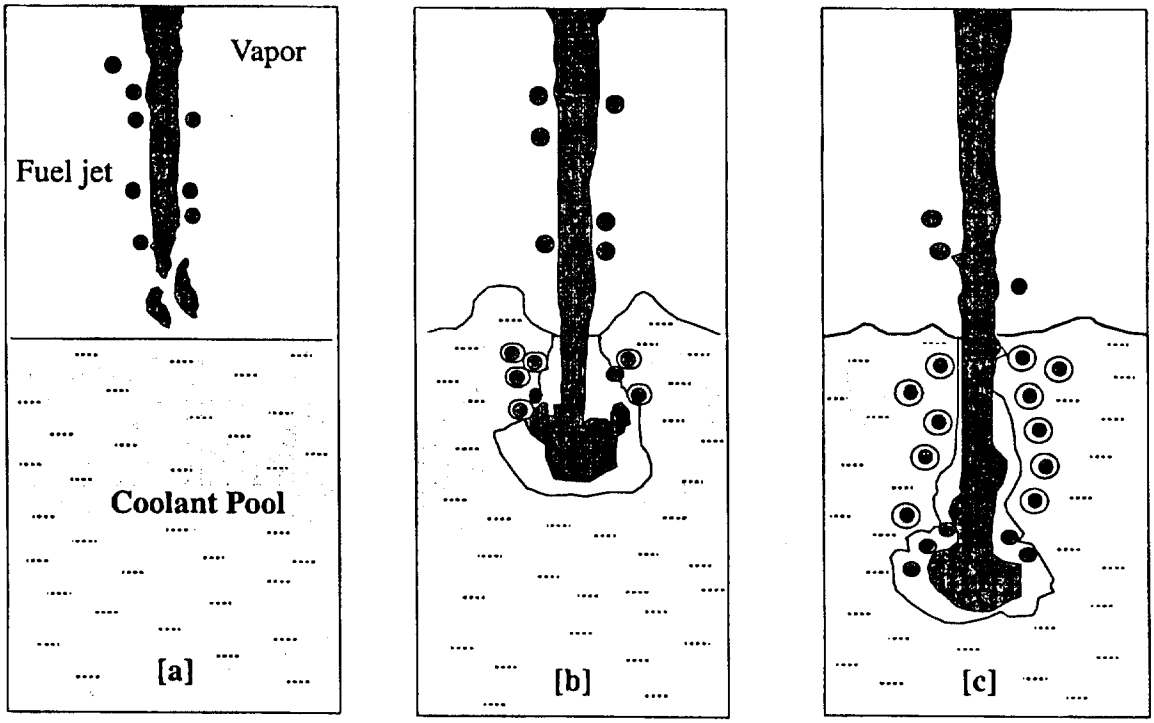


[a] Fuel jet encouters modest breakup in vapor region
[b] Fuel jet leading edge grows due to stagnation flow
[c] Fuel jet breakup at leading edge and along jet body

**Figure 2.** Schematic of the molten fuel jet break-up.

Figure 3 shows general flow conditions and jet breakup regimes as given by Ginsburg (1986) and Bürger et al. (1995). First regime (A-B) is Rayleigh regime in which an axisymmetric, varicose disturbance grows as a function of distance from the jet exit. The pressure and surface tension forces interact to break-up the jet into droplets. The B-C regime is called "transition" or "first wind" and depends on the ambient system pressure, and turbulence. The third regime (C-D) is called turbulent or "second wind," although there may be no turbulence in the jet. The Reynolds number is of the magnitude that causes turbulent flow in a pipe. According to some researchers, capillary wave growth and eventual stripping of droplets from the jet surface are the main reasons for droplet formation. However, major cause of the bulk jet breakup is still not well understood.

There may be a transverse disturbance, which grows in amplitude, stretching and thinning the jet at some locations until the jet breaks into droplets. The regime D-E is associated with a small jet diameter (usually < 1 mm), high velocity (> 100 m/s), and large Weber number. Also, the shape of the curve D-E is not certain. It is highly unlikely that the molten fuel jet falling into the lower plenum will fall in this regime.

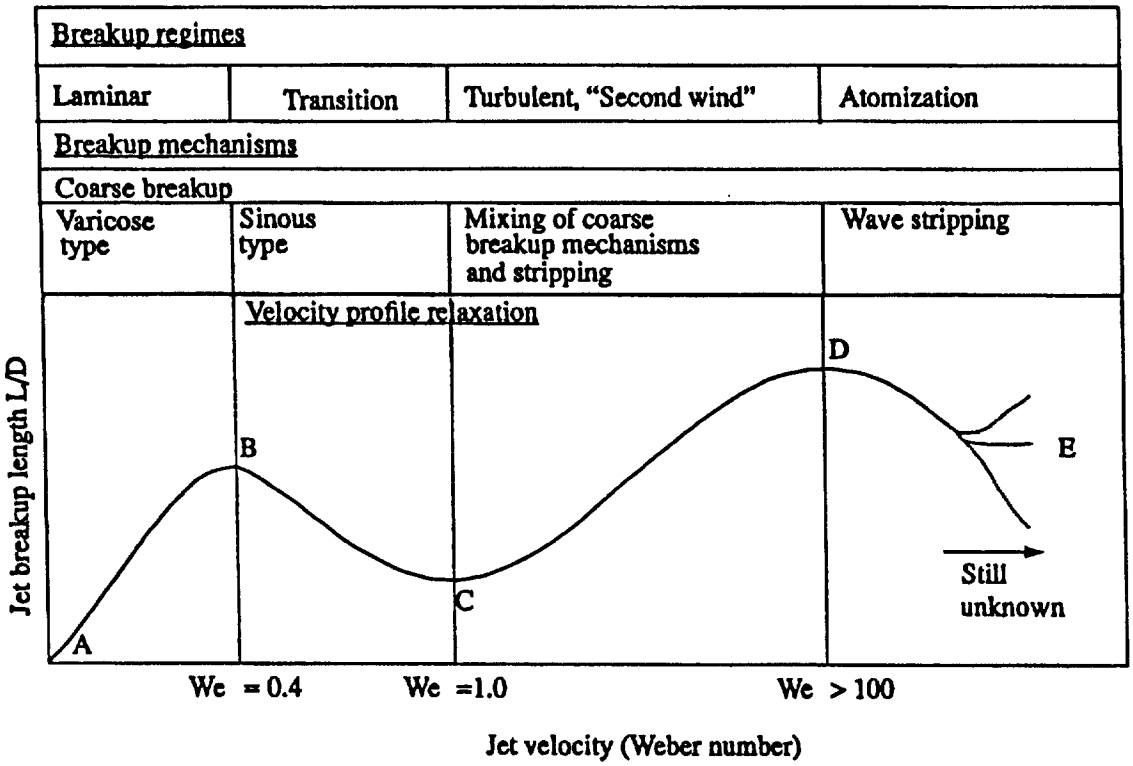


**Figure 3.** Jet break-up length curve with related break-up regimes and mechanisms. Bürger, et al. (1995)

Theofanous and Saito (1982) have examined the phenomena of liquid jet breakup and melt-coolant mixing. They concluded that fluid dynamic effects of water surrounding the molten fuel jet possibly account for jet break-up and mixing. Epstein and Fauske (1985) further examined these phenomena including the effects of film boiling on break-up as shown in Figure 4. They considered the jet break-up under two bounding conditions of (a) thin vapor film, and (b) thick vapor film. In thin film case, the water density (or liquid flow) determines the breakup behavior, whereas in the thick film case, the steam density (or vapor flow) determines the melt stream breakup behavior. They also assumed a steady-state jet breakup, which means that the jet breakup and mixing that would occur at the leading edge as the jet first enters the coolant pool is neglected. The details of the interfacial instability analysis are given by Chandrasekhar (1961).

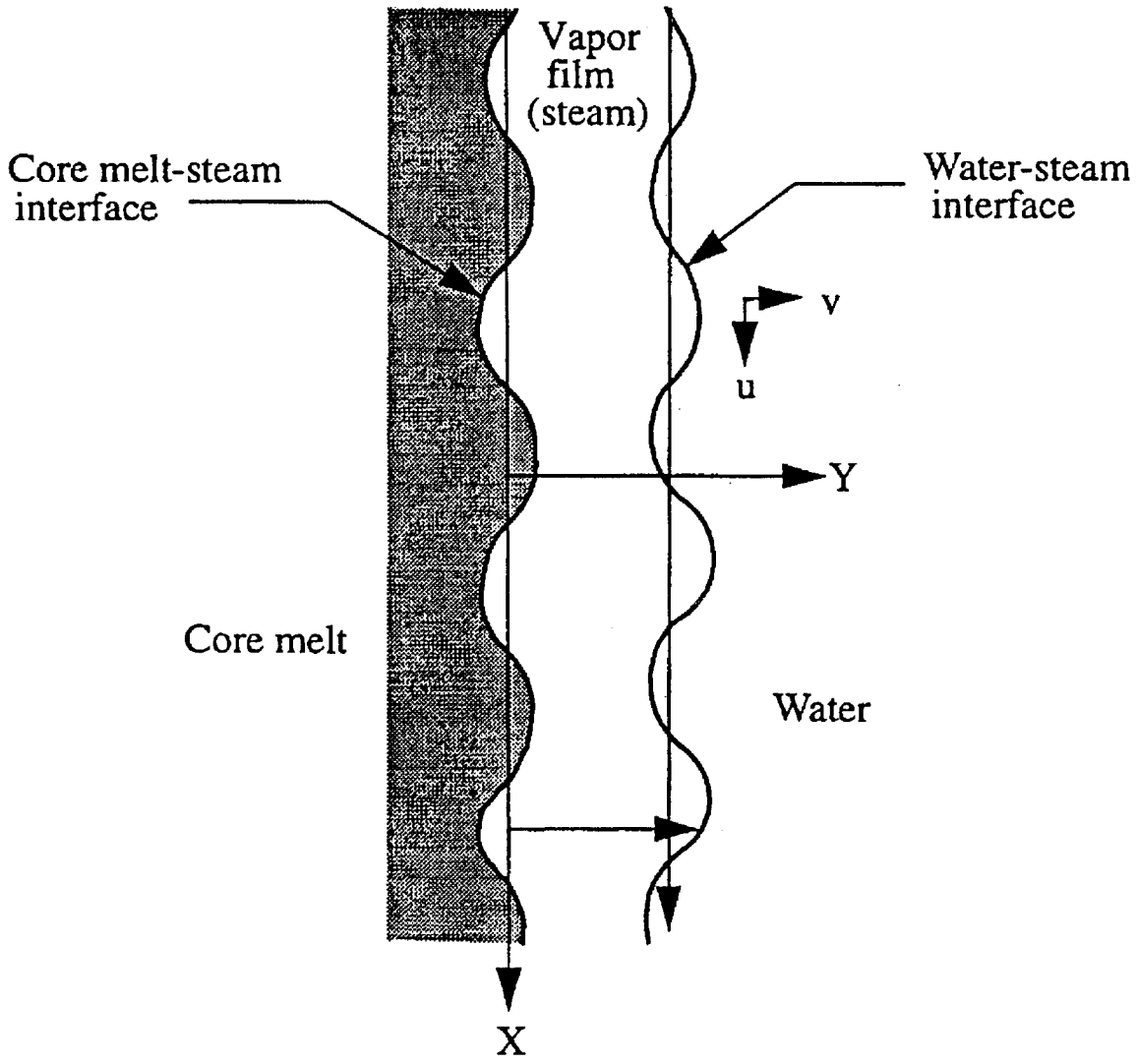


**Figure 4.** Schematic of melt-stream and stream-water interface stability model. (Epstein and Fauske, 1985)

Recently, Bürger et al. (1995) have also reviewed the currently available models for break-up of melt jets. Their model is based on the lateral stripping of the droplets from the jet by considering relative effects of Kelvin-Helmholtz (K-H) instability and shear flow induced waves at the jet surface, and coarse breakup at the leading edge of the jet. Recently, Chu, et al. (1995) have also given a detailed and comprehensive description of the various mechanisms responsible for the molten fuel jet breakup. The most comprehensive model developed to-date has been by Corradini and co-workers (1997) at the University of Wisconsin. In their model, they have incorporated all three types of mechanisms responsible for the fuel break-up and are described below in detail.

Figure 2 (a-c) shows a mechanistic view of molten jet entering the coolant in the lower plenum and breaking into droplets. Most of the researchers agree that various types of hydrodynamic instabilities and fluid-fluid interactions cause the jet breakup. Another mechanism responsible for drop formation is boundary layer stripping. Each mechanism is dominant under a particular set of conditions. Corradini, et al. (1997) have based their model on the experimental observations by Hohmann et al. (1995). Initially, because of relative velocity between the jet and the vapor, small melt droplets are stripped off the jet surface. The leading edge of the jet is deformed into a "mushroom-like" shape as it penetrates the coolant. The dynamic pressure and the shear force between the jet and the coolant cause the melt flow from the front stagnation point to the rear of the "mushroom-like" leading edge and in the process gets stripped off. This process is called the boundary layer stripping and is confined to only the leading edge. As the jet penetrates the coolant, the waves with a short wavelength at the surface of the jet (upper section above the leading edge) grow and become unstable due to the K-H instability. The unstable wave causes melt droplets to form. Large relative velocity between the fluids results in small droplets (< 1 mm) and vice versa. If the wavelength of the instabilities becomes large, the jet column near the leading edge would break-up into large discrete "lumps" due to R-T instability. Depending on the coolant volume and temperature, and the jet Weber number, the breakup into droplets will continue until stable size debris are formed and settled at a location in the coolant.

Chu (1986), and Chu and Corradini (1989) have modeled the molten fuel breakup as it penetrates the coolant in the lower plenum and the model is called TEXAS. Besides modeling break-up, they have also modeled the thermal hydraulics of the jet and the surrounding fluids, heat transfer between various interacting fluids and plenum walls.

# 2. AVAILABLE FCI MODELS

Several research groups at nuclear reactor related research centers around the world have developed models to represent the molten fuel-coolant interaction. Therefore, it was decided to make use of the available models as much as possible. Considering a few rule of thumb criteria (availability, relevance, compatibility, and ease of implementation), following six codes were evaluated for their suitability for incorporating in SCDAP/RELAP5. For detailed description of the codes, the readers are referred to the respective references.

## 2.1 FCI Models

1. CHYMES - Fletcher and Thyagaraja (1991) of Culham Laboratory, AEA Technology, Abingdon, Oxfordshire, England developed a transient, two-dimensional code called CHYMES to model the mixing of fuel melt and coolant. They also developed a model, CULDESAC (Fletcher, 1995) to analyze the wave propagation in the melt droplets, steam, and water mixture.

2. IFCI – Young (1987) at Sandia National Laboratories developed a code IFCI, which is an extension of the models in the FLUIDS module in the MELPROG/MOD1 code, which is a code to calculate the events occurring during a hypothetical reactor core meltdown accident.

3. K-FIX and PM-ALPHA - Theofanous and coworkers at the University of California, Santa Barbara (Abolfadl and Theofanous, 1987) used a code K-FIX developed by Rivard and Torrey (1977) at the Los Alamos National Laboratory to calculate premixing of the molten-fuel and coolant. Amarsooriya and Theofanous (1991) modified the K-FIX code to develop a code PM-ALPHA. The propagation of the mixture was modeled by a code ESPROSE (Medhekar et al., 1989).

4. SIMMER-II – Bohl (1990) at the Los Alamos National Laboratory improved thermophysical properties and heat transfer correlations in SIMMER-II code to calculate molten core -coolant interaction. In this code the fuel and the coolant have the same velocity (no slip condition). SIMMER-II code used a prefragmented fuel for use in the surface boiling model, which gives an increased pressure in the FCI region.

5. TEXAS – Chu (1986), and Chu and Corradini (1989) at the University of Wisconsin, Madison developed a code TEXAS to model the FCI phenomena. Initially, TEXAS was a one-dimensional version of the IFCI code. It is a transient, three fluid, one-dimensional code with two Eulerian fields for coolant liquid and vapor, and one Lagrangian field for fuel droplets. The code allows thermal and mechanical nonequilibrium between coolant liquid and vapor. The Lagrangian treatment of the fuel droplets makes it easier to track the movement of the fuel droplets. The code calculates the heat transfer between the fuel and the coolant under different conditions and flow regimes. Initially in TEXAS-II, Chu and Corradini (1989) had modeled the fuel fragmentation based on only Rayleigh-Taylor (R-T) instability. However, recently in TEXAS-V (Corradini, et al., 1997), contributions by all three mechanisms (R-T, K-H, and boundary layer stripping) have been included. These modifications have improved the code predictions with the experimental data.

6. THIRMAL-1 - Chu, et al. (1993, 1995) at the Argonne National Laboratory have developed a code THIRMAL-1 to calculate the nonexplosive interactions that occur when corium enters a water pool as a coherent melt stream. It models the breakup of a coherent melt stream due to the growth of the instabilities along the stream surface. It models the melt droplets in a Lagrangian manner and surrounding water and steam are modeled by Eulerian representation. A one-dimensional formulation of the flow of water and steam is employed in the mixing zone, the region surrounding the melt stream and melt droplets.

### 2.2 Selection of FCI Models/Submodels

The selection of one code or model over another one is not a matter of one being better than the other. It is more of making a choice from several possibilities and selecting one that most closely meets the stated objectives. Based on the criteria established, many available FCI codes were found unsuitable for incorporation in SCDAP/RELAP5 code. Initially, TEXAS code was developed by Chu and Corradini at the University of Wisconsin, Madison. Although the source code is not available free of cost, the basic information is available in detail from Chu's Ph.D. thesis (Chu, 1986). Basic TEXAS governing equations and code manual are also available at a web-site, http://elvis.neep.wisc.edu/nsrc/. TEXAS is a one-dimensional code, which is compatible

with RELAP5. The code has been recently upgraded to TEXAS-V. TEXAS has been used by the researchers at Joint Research Center, Ispra, Italy to plan for their experiments. Also, TEXAS predictions have been tested against the experimental data. Actively upgrading, availability of the basic governing equations, and availability of the principal researcher for any assistance, make TEXAS code as an ideal choice for our purpose. Presently, the TEXAS code is being converted into a three-dimensional code. The governing equations and constitutive correlations from published literature on TEXAS-V for fuel melt break-up were implemented in SCDAP/RELAP5. The Lagrangian formulation for molten fuel jet break-up, movement of fuel droplets in the coolant, corresponding momentum and energy exchange can be coded and solved in conjunction with RELAP5 thermal hydraulics. Therefore, only the models for fuel jet breakup and Lagrangian description of droplets from TEXAS-V were used to couple with RELAP5 thermal hydraulics. Some of these governing equations are described below.

# 3. SELECTED FCI MODELS

The model selected is described in the form of equations and a brief discussion on its implementation in SCDAP/RELAP5 is presented. Although detailed TEXAS code models are published elsewhere, salient features are presented here for completeness of the paper.

## 3.1 Liquid Jet Breakup Model

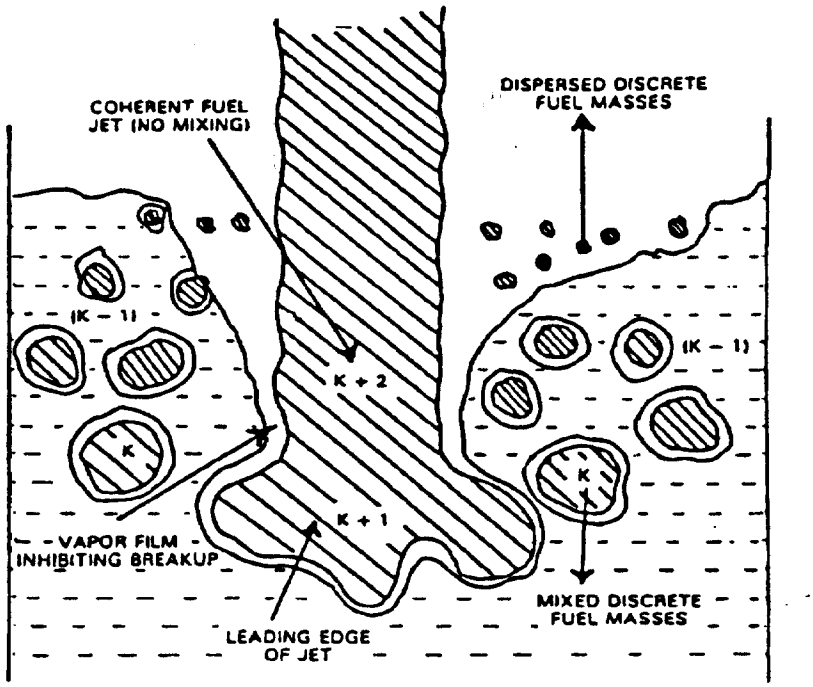


**Figure 5.** Schematic of molten fuel jet and water mixing model. (Chu, 1986)

Chu and Corradini (1989) and Corradini et al. (1997) developed a liquid jet breakup model as shown in Figure 5 and incorporated it in the TEXAS-V code. The three mechanisms responsible for the molten fuel breakup into the droplets are (1) boundary-layer stripping at the jet "leading edge," (2) Kelvin-Helmholtz (K-H) instability causing jet surface erosion, and (3) Rayleigh-Taylor (R-T) instability causing further fragmentation of discrete droplets already broken off from the jet. The fuel jet is assumed to enter the coolant as a series of discrete masses (globules) or as a molten jet or both. The model user is required to specify the diameter, velocity, and temperature of the liquid jet.

As a molten fuel jet enters the water pool and decelerates, first the "leading edge" breaks up according to the dynamic breakup model and the resulting droplets are swept away, a process called boundary layer stripping. The analysis for boundary layer stripping is done by assuming that in the moving frame of the "leading edge" of the molten fuel jet, the melt velocity at the melt-coolant interface is approximately equal to the relative velocity between the "leading edge" and the coolant. The mass flow rate of the fuel removed by boundary layer stripping, $M_{BLS}$, can be calculated as

$$\frac{dM_{BLS}}{dt} = \rho_p \int_{(R-\delta)}^{R} 2\pi U r dr \qquad (1)$$

The integration of Equation (1) yields

$$\frac{dM_{BLS}}{dt} = \rho_p [2\pi U_0 \delta (\delta - 0.31606 R) \pi R^2] \qquad (2)$$

To use the boundary layer stripping model, Corradini et al. (1997) recommended that the fuel mass within the leading edge should be taken equal to two Lagrangian master particles, although its exact value does not make a significance difference in the final calculations. The droplets are formed from the jet leading edge because of boundary later stripping with diameter equal to *. These droplets can further breakup by R-T instability criterion given by Equation (10). The discrete mass, K, as shown in Figure 5, eventually breaks up into smaller discrete masses (K-1) and this process continues for droplets belonging to a particular size group in any computational cell. The smallest stable droplet diameter as a result of this stepwise fragmentation can be determined by the critical Weber number.

$$D_{BLS} = We_{crit}\, \sigma_p/(\rho_c U_{rel}^2) \qquad (3)$$

In implementing the FCI model into SCDAP/RELAP5, it was assumed that the leading edge is stationary, $U_0 = 0.0$. This assumption results in the calculation of no breakup due to boundary layer stripping. The effect of K-H instability is considered dominant along the body of the jet, where K-H waves develop because of relative velocity between the fuel jet and the surrounding fluid. According to Corradini, et al. (1997), the melt erosion rate, $M_{KH}$, is proportional to the increase in volume flux of the waves growing on the jet surface. The volume

flux is approximately equal to the product of growth speed of the wave, $n\lambda$, and the cross-sectional area of a wave, $C_0\lambda^2$. The waves grow up to be broken as droplets. Corradini et al. (1997) have given the mass erosion rate by K-H instability of one wavelet as

$$dM_{KH}/dt = \lambda^2 (n\lambda) \rho_p \tag{4}$$

The total erosion rate for a jet surface area can be obtained by

$$dM_{KH}/dt = C_0 A (n\lambda)_{max} \rho_p \tag{5}$$

The terms $n_{max}$ and $\lambda_{max}$ are determined using the analysis given by Epstein and Fauske (1985) and the corresponding phenomenon is shown in Figure 4. The maximum growth wavelength of a disturbance, $\lambda_{max}$, is related to the minimum wave number, $k_{min}$, as $\lambda_{max} = 2 \lambda \pi / k_{min}$. Two bounding conditions are used, which are based on the condition of the continuous fluid surrounding the fuel jet. If the continuous fluid is mostly liquid (void fraction < 0.2), the condition of "thin film" is used. If the continuous fluid is a mixture of liquid and vapor (void fraction > 0.2), the condition of "thick film" is used. According to Corradini, break-up of the jet into droplets is not too sensitive to the value of the void fraction (0.2 to 0.5) chosen for transition from thin film to thick film.

For a thin film case,

$$n_{max}^2 = \rho_p \rho_L k_{min}^2 \frac{(u_L - u_p)^2}{(\rho_p + \rho_L)^2} - k_{min}^3 \frac{(\sigma_p + \sigma_L)}{(\rho_p + \rho_L)} \tag{6}$$

where

$$k_{min} = \frac{2\rho_p \rho_L (u_L - u_p)^2}{3(\rho_p + \rho_L)(\sigma_p + \sigma_L)} \tag{7}$$

For a thick film case,

$$n_{max}^2 = \rho_p \rho_g k_{min}^2 \frac{(u_g - U_p)^2}{(\rho_p + \rho_g)^2} - k_{min}^3 \frac{\sigma_p}{(\rho_p + \rho_g)} \tag{8}$$

where

$$k_{min} = \frac{2\rho_p \rho_g (u_g - u_p)^2}{3(\rho_p + \rho_g)\sigma_p} \tag{9}$$

Initially, the eroded mass forms droplets with diameter equal to $\lambda_{max}$ and can further breakup according to the R-T instability criteria given in Equation (10).

Chu (1986) developed the theoretical model for R-T instability and the model was simplified as a linear correlation of the theoretical model. Thus, for the fuel entering the coolant initially as a "globule" or the droplets broken off from the jet, the diameter of the droplet at a new time step (n+1), is calculated as follows.

$$D_p^{n+1} = D_p^n (1-C_1 \Delta t_b We^{0.25}) \quad (10)$$

In implementing the FCI model, it was assumed that droplets split into two particles when $D_p^{n+1}$ attains a value such that two droplets with diameter $D_p^{n+1}$ equal the mass of the droplet before splitting. Thus, a droplet is calculated to split during a time step when the following criterion is satisfied.

$$D_p^{n+1} \le \left(\frac{1}{2}\right)^{0.333} D_p^n \quad (11)$$

### 3.2 Model for Heat Transfer Between the Fuel Droplets and the Coolant

Prior to settling at the lower plenum bottom, the heat transfer between the fuel particles and the plenum walls is being neglected because it is estimated to be small compared with the heat transfer to the coolant. To calculate the heat transfer between the fragmented fuel droplets and the surrounding fluid, the droplets are modeled as "mobile SCDAP heat structures." A mobile heat structure is defined for each unique collection of drops that are created by FCI. It means that a heat structure with surface area equivalent to that of a group of droplets will be modeled. The motion of the droplets is calculated using a Lagrangian framework.

The heat transfer between the droplets and the surrounding fluid is based on the model used by Chu (1986) in the TEXAS code, the details of which are given in Chapter 4.1.4 of Chu's thesis. The molten fuel jet and the droplets are surrounded by either water or steam. At any time step, in a computational cell, the newly formed droplets and the liquid jet are at the same temperature and therefore, do not exchange energy. The droplets formed at an earlier time step may have a temperature lower than that of the fuel jet and will be governed by the following heat transfer mechanism. In one scenario, shown in Figure 6, the liquid droplets may be surrounded by a blanket of vapor film and both may be surrounded by continuous liquid. In such a case, the fuel droplet transfers heat mainly by convective film boiling and radiation to the surrounding liquid. However, if the vapor film breaks loose from the fuel droplets and forms one large bubble or many small bubbles, the heat transfer from the bubble occurs by conduction to the vapor-liquid interface (between the vapor bubble and the continuous liquid) and by convection to the continuous liquid. In a second scenario, the fuel droplets may be dispersed in continuous vapor. In this situation, heat transfer from the fuel droplets is by convection to the continuous vapor and by radiation to water droplets. However, it has been assumed here that major heat transfer is from the fuel droplet to the liquid and is used in evaporating liquid and does not transfer heat to vapor or water droplets, if any. The heat transfer from vapor to water being small has been neglected. These assumptions are used to make reduce the computations time and may

be revisited if the model does not compare satisfactorily during model assessment.

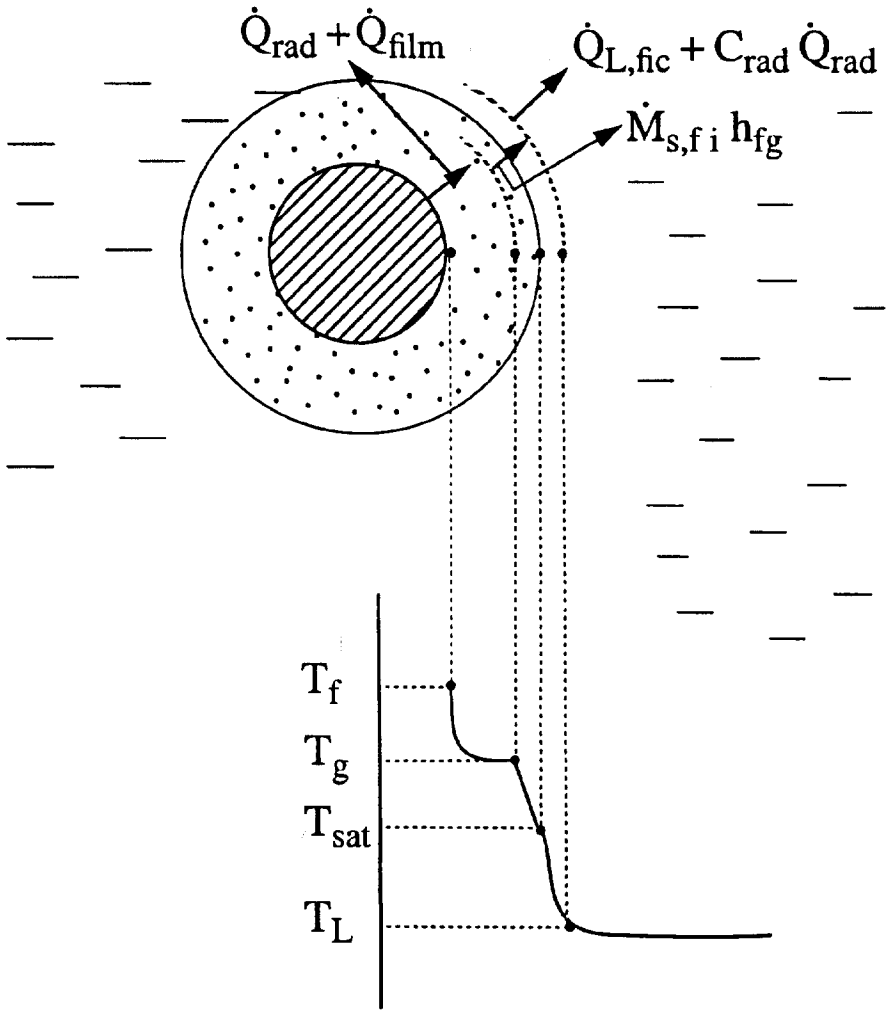


**Figure 6.** Model of heat transfer from fuel droplet to surrounding fluid. (Chu, 1986)

In the first situation, when the fuel droplet is surrounded by vapor film and continuous liquid, the heat transfer rate from the fuel droplet to the surroundings can be defined as:

$$\dot{Q}_p = \dot{Q}_{film} + \dot{Q}_{rad} = \pi D_p^2\, h_{film}\,(T_p - T_{sat}) + \pi D_p^2\, h_{rad}\,(T_p - T_{sat}) \qquad (12)$$

The convective film boiling heat transfer coefficient, $h_{film}$, around a sphere is taken from the correlation developed by Dhir and Purohit (1987).

$$h_{film} = \mathrm{Max}\left(h_{free}, h_{forced}\right) \qquad (13)$$

Terms on the right hand side of Equation (13) are evaluated by the following relations.

$$h_{free} = h_{sat} + h_{nc}\frac{\Delta T_{sub}}{\Delta T_p} \tag{14}$$

In Equation (14), $h_{sat}$ is saturated free convection film boiling heat transfer coefficient averaged over a sphere. It is a modification (Dhir and Purohit, 1987) of the correlation given by Bromley et al. (1953) for horizontal cylinders by changing the numerical multiplier from 0.62 to 0.8 and disregarding the radiation heat transfer and is given by the following relation.

$$h_{sat} = 0.8\left[g\rho_g k_g^3 h_{hfg}\frac{(\rho_L - \rho_g)}{D_p \Delta T_p \mu_g}\right]^{0.25} \tag{15}$$

The natural convection heat transfer coefficient averaged over a sphere (fuel droplet), $h_{nc}$, and forced convection film boiling heat transfer coefficient is given by the following relations.

$$h_{nc} = 0.9\left[g\rho_L^2 k_L^3 C_{pL}\beta\frac{\Delta T_{sub}}{(D_p \mu_L)}\right]^{0.25} \tag{16}$$

$$h_{forced} = h_{sat} + 0.8\,Re^{0.5}\left[1 + \frac{\Delta T_{sub}}{\Delta T_p}\left(\frac{k_L}{k_g}\right)\right]\frac{k_g}{D_p} \tag{17}$$

The temperature of the dispersed droplets is calculated by two methods. The first method is used when the droplet is at a temperature above its solidus temperature. In this case, the heat transfer and changes in internal energy of the material are rapid. The second method is used when the droplets are at a temperature lower than the solidus temperature. In this case, an equation for the transient temperature of a small particle at a uniform temperature is solved.

As in Equation (12), total heat transfer coefficient from a particle is given by the sum of heat transfer coefficients for film boiling convection heat transfer and radiation heat transfer coefficient.

$$h_{tot} = h_{film} + h_{rad} \tag{18}$$

$$\frac{1}{6}\pi D_p^3 \rho_p \frac{(E_p^{n+1} - E_p^n)}{\Delta t} = \frac{1}{6}\pi D_p^3 q_p - \pi D_p^2 h_{tot}(T_p^n - T_{sat}) \tag{19}$$

The particle temperature, $T_p^{n+1}$, can be calculated as a function of $E_p^{n+1}$. In the second case for, $T_p^n < T_s$, the droplet temperature can be calculated by solving the following heat balance

equation

$$\frac{1}{6}\pi D_p^3 \rho_p c_p \frac{dT_p}{dt} = \frac{1}{6}\pi D_p^3 q_p - \pi D_p^2 h_{tot} (T_p - T_{sat}) \tag{20}$$

With an initial condition, $T_p = T_p^n$, at $t = t^n$, solution of Equation (20) can be written as,

$$T_p^{n+1} = C_a + (T_p^n - C_b) e^{-C_b \Delta t} \tag{21}$$

where

$$C_a = \frac{\frac{1}{6} D_p q_p + h_{tot} T_{sat}}{h_{tot}}, \text{ and} \tag{22}$$

$$C_b = \frac{h_{tot}}{\frac{1}{6} D_p \rho_p c_p} \tag{23}$$

The momentum change of the dispersed particles is calculated taking into account acceleration due to gravity and the drag exerted by the fluid. The rate of change of particle velocity (acceleration) is calculated by the following equation.

$$\frac{du_p}{dt} = g - \frac{F_p}{\frac{1}{6}\pi D_p^3 \rho_p} \tag{24}$$

The drag force, $F_p$, is the sum of drag forces caused by the liquid and vapor phases. These can be calculated by the following equations.

$$F_{pL} = \frac{f_L}{8}\pi D_p^2 (1-\alpha_g) \rho_L (u_L - u_p)^2 \tag{25}$$

$$F_{pg} = \frac{f_g}{8}\pi D_p^2 \alpha_g \rho_g (u_g - u_p)^2 \tag{26}$$

The friction factors are functions of Reynolds number based on the relative velocity between the particle and the liquid or vapor.

## 4. TESTING OF THE SELECTED FCI MODEL

The selected fuel-coolant interaction (FCI) model was assessed by using the results of two FCI experiments and by performing a sensitivity study of the effect of the number and size of the slumping material jets on the FCI phenomenon. First FCI experimental data used for the assessment were obtained by Angelini, et al. (1995) in a MAGICO-2000 series of experiments. The second set of experimental data for assessment was obtained by Hohmann et al. (1995) at the Joint Research Center, Ispra, Italy. The third test problem involved a study of the effect of the number and size of jets of slumping material on the FCI that occurs under conditions typical of those on a PWR during a severe accident.

### 4.1 Assessment with a MAGICO-2000 Experiment

An experiment identified as Run Z1500/0.2 in the MAGICO-2000 series of experiments performed at the University of California at Santa Barbara, California was used to assess the validity of the FCI model. This experiment involved slumping of a cloud of small hot particles made of $ZrO_2$. The characteristics of the experiment are given in Table 1.

In this experiment molten fuel jet did not interact with water, instead hot particles were dropped in a pool of water. From this experiment three values are compared with those from the current FCI model. These values are: (1) void fraction for a small period of time at one location in the test facility, (2) location of the cloud of particles as a function of time, and (3) transient

**Table 1.** Characteristics of Run Z1500/0.2 of MAGICO (Angelini et al., 1995) and Test L-08 of FARO (Hohmann et al., 1995) Experiments.

| Parameter | Value (MAGICO) | Value (FARO) |
|---|---|---|
| Initial height of column of water (m) | 0.8 | 1.0 |
| Diameter of test vessel (m) | 0.6 | 0.71 |
| Diameter of jet nozzle (only for FARO experiment) (m) | - | 0.1 |
| Distance of free fall of particles/jet (distance from initial position to initial surface of water (m) | 1.2 | 1.53 |
| Volume of gas ($H_2O$, Ar) above water surface ($m^3$) | - | 0.875 |
| Initial pressure in test vessel (MPa) | 0.1 | 5.8 |
| Initial temperature of column of water (K) | | 536 |
| Water subcooling (K) | 0.0 | 10 |
| Velocity of particles/jet at surface of water (m/s) | 4.8 | ~10 |
| Initial temperature of particles/jet material (K) | 1648 | 3023 |
| Mass of particles/slumped material (kg) | 6.2 | 44 |
| Pour equivalent diameter (m) | 0.225 | |
| Pour duration (s) | 0.33 | 0.37 |
| Chemical composition of particles/jet material | $ZrO_2$ | $UO_2$ (80%) + $ZrO_2$ (20%) |

swell of water level. The calculated and measured locations of the front of the cloud of plunging particles are compared in Figure 7. The good agreement of calculations with the measurements indicates that the FCI model correctly calculates the motion of the particles under gravitational and drag forces. The calculated and measured liquid void fraction in the test vessel at a location 0.65 m above the bottom of the test vessel are compared in Figure 8. The experiment measured only one data point at 0.45 s after dropping the hot particles. The calculated value of liquid void fraction is significantly higher than the measured value. One reason for this discrepancy may be lower heat transfer rate resulting in lower volume of vapor generation during first 0.5 s of the FCI. Higher vapor velocity (0.2 m/s) can also lead to higher value of liquid void fraction. The calculated and measured water swell levels as functions of time are compared in Figure 9. The upper and lower bounds of measured water level correspond to the liquid void fractions of 0.5 and 0.1, respectively. As shown in Figure 9, the approximate agreement of the calculations with the measurement indicates that the calculations for heat transfer between the particles and the coolant are reasonable.

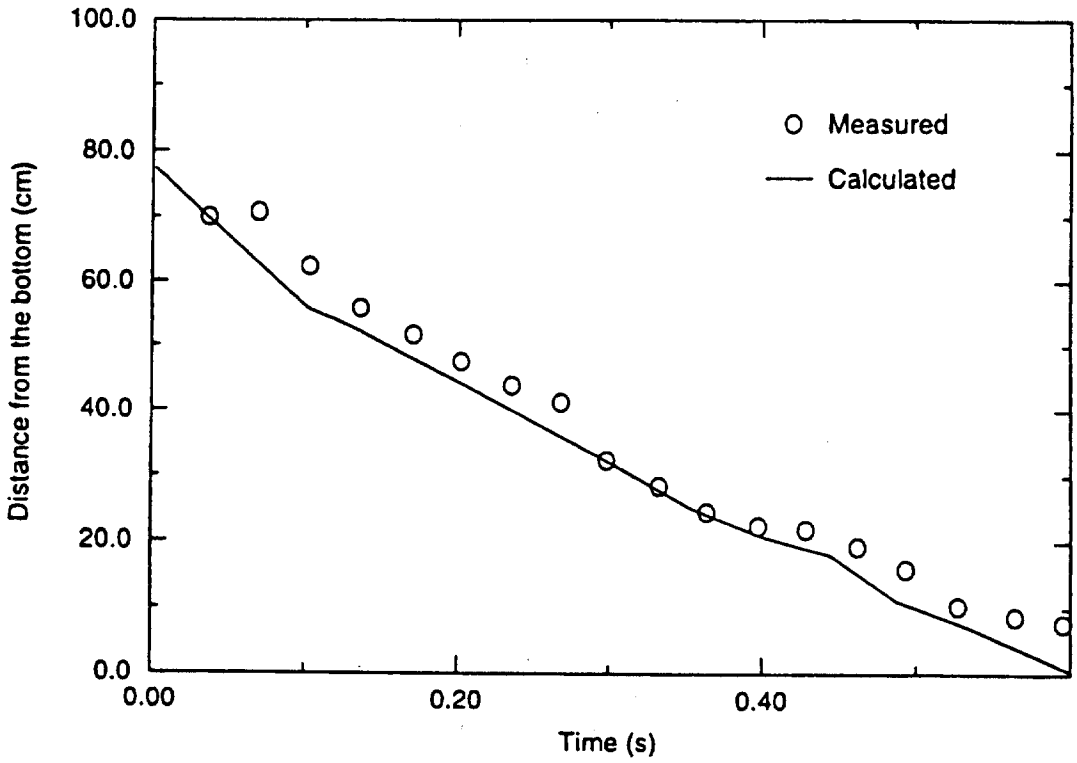


**Figure 7.** Comparison of Calculated and measured front of the particles for MAGICO-2000 experiment.

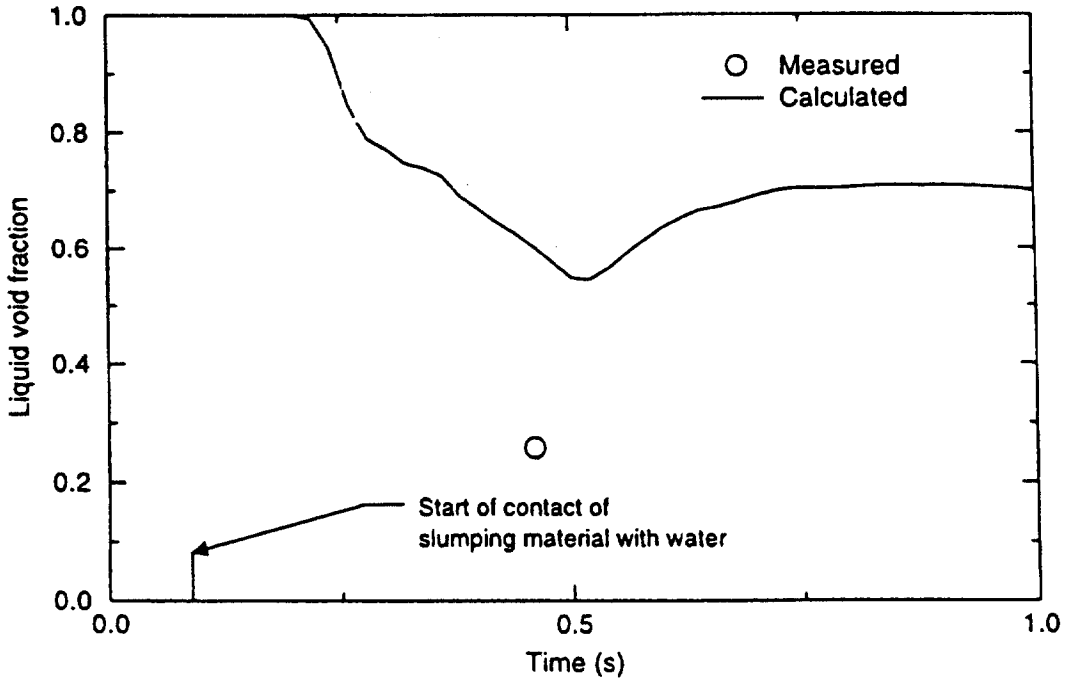


**Figure 8.** Comparison of calculated and measured liquid void fraction ($1-\alpha_g$) at an elevation of 0.65 m for MAGICO-2000 experiment.

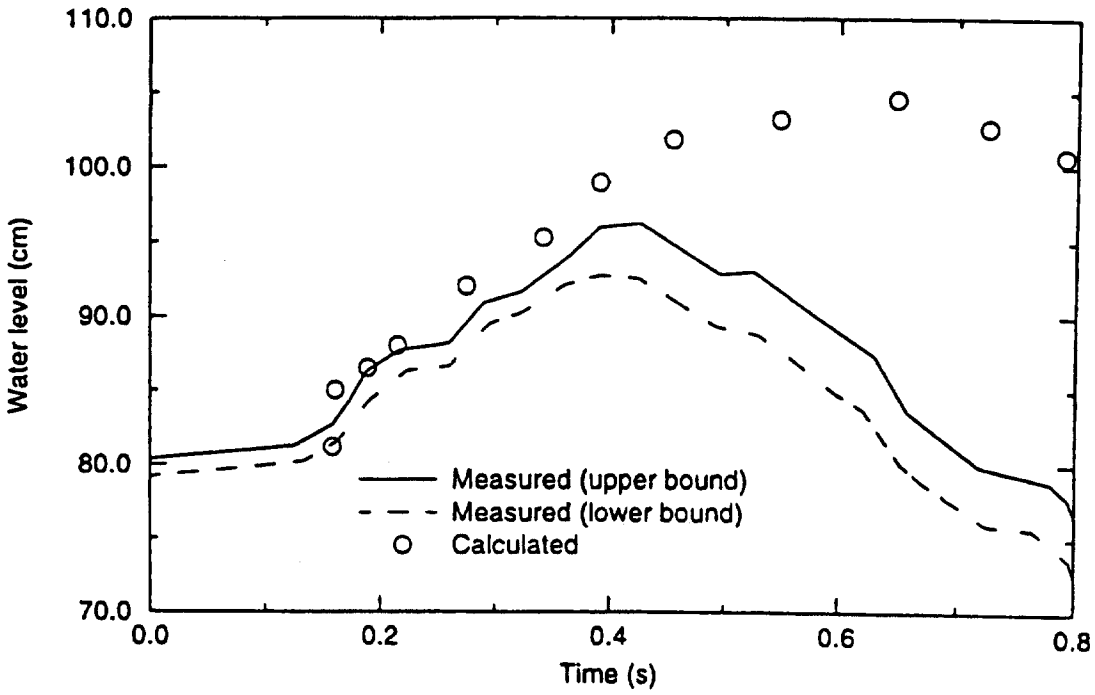


**Figure 9**. Comparison of calculated and measured water level swell for MAGICO-2000 experiment.

### 4.2 Assessment with a FARO Experiment

An experiment, Test L-08, performed in the FARO series of experiments (Hohmann et al., 1995) was used to assess the capabilities of the FCI model to calculate the break-up of a jet of molten material that plunges into a column of water and heat transfer between the material and water. The characteristics of the FARO test are shown in Table 1. Four experimental measurements were compared with the calculations. These are: (1) transient pressure in the test vessel, (2) fraction of break-up of the jet of molten material, (3) size of particles resulting from break-up, and (4) transient temperature of the plate onto which the slumping material settled.

The calculated and measured pressures in the test vessel are compared in Figure 10. Although the two pressure histories show the same trend, the calculated rate of pressure increase during first 1 s is ~13.5% lower than the corresponding measured value. After initial 1.5 s, the calculated pressure increase and the corresponding measured value are in good agreement. A summary of the measured and calculated data is shown in Table 2. The break-up model calculates that 73% of the slumping jet breaks into particles, which is nearly the same as the measured value of 68%. The mean diameter of the broken-up material based on weight was calculated to be 2.8 mm, which is smaller than the measured value of 3.8 mm. The calculated and measured values of temperature increase of bottom plate are 352 and 275 K, respectively. The level swell of water is an indication of vapor generated. The calculated and measured values of level swell of water are 0.25 m and 0.15 m, respectively.

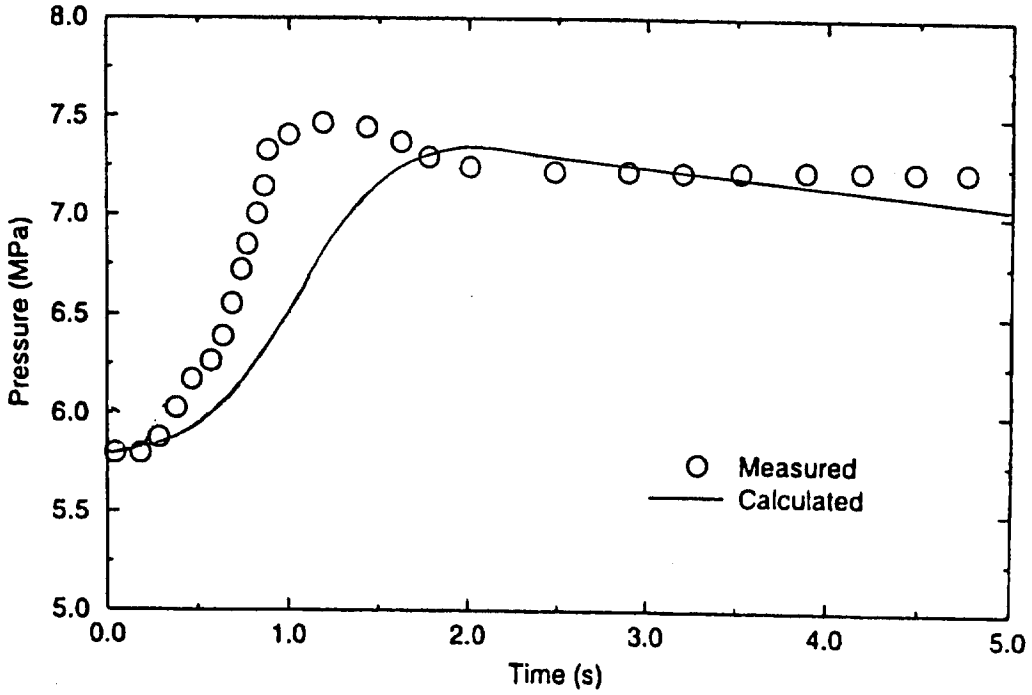


**Figure 10**. Comparison of calculated and measured pressure rise for FARO Test L-08.

**Table 2.** Summary of measured and calculated parameters for FARO Test L-08.

| Parameter | Measured | Calculated |
|---|---|---|
| Fraction of break-up of slumping material | 0.68 | 0.73 |
| Mean particle diameter of broken-up material based on mass (mm) | 3.80 | 2.80 |
| Maximum pressure increase caused by FCI (MPa) | 1.70 | 1.50 |
| Maximum temperature increase of bottom plate (K) | 2.75 | 3.52 |
| Level swell of water (m) | 0.15 | 0.25 |

The most significant discrepancy is between calculated and measured values of mean particles size resulting from break-up of the slumping material. The calculated size is smaller than the measured size, which results in larger heat transfer surface area. Hence, more vapor is generated, which leads to rapid increase in calculated pressure. One possible reason for this discrepancy may be the use of incorrect value of interfacial surface tension (0.45 N/m) between a mixture of $UO_2$ and $ZrO_2$, and water. The upper limit for this property is ~1.45 N/m, which will significantly increase the mean particle size. Another possible reason may be higher prediction of the steam velocity, which results in higher break-up rate and smaller particle size.

### 4.3 Examples of Application of FCI Model to Severe Accident Analysis

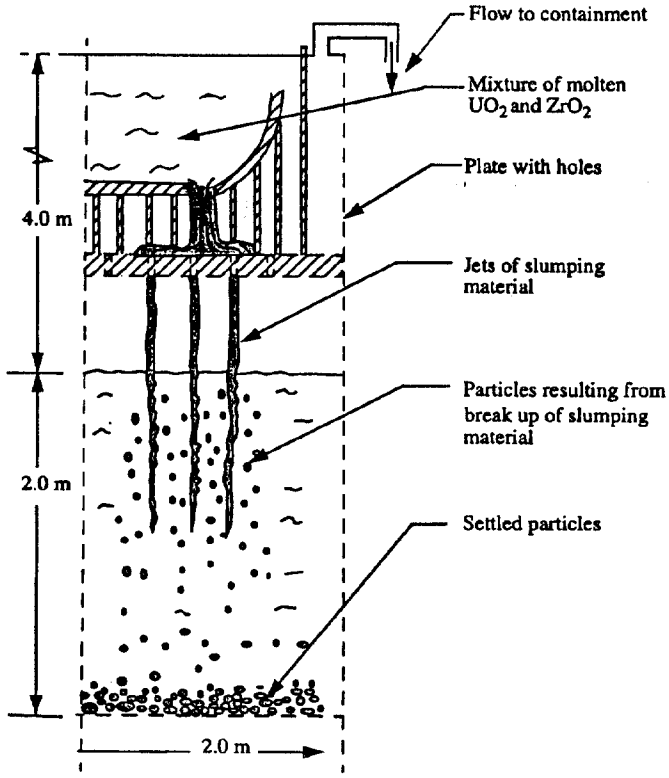


**Figure 11.** Schematic of application of FCI model to severe accident analysis.

The FCI model was applied to five hypothetical, but possible cases of severe accident situations in a pressurized water nuclear reactor (PWR). The number and diameter of slumping material jets depend on a specific case. Therefore, a few representative cases are being analyzed here. In each case, a core meltdown in a PWR is assumed to have occurred that results in molten material slumping into a pool of water in the lower head of the reactor vessel as shown in Figure 11. Table 3 shows various parameters related to all the cases.

**Table 3.** Parameters for five cases of severe accident with possibility of FCI

| Parameters | Case 1 | Case 2 | Case 3 | Case 4 | Case 5 |
|---|---|---|---|---|---|
| Initial height of column of water (m) | 2.0 | 2.0 | 2.0 | 2.0 | 2.0 |
| Diameter of vessel (m) | 2.0 | 2.0 | 2.0 | 2.0 | 2.0 |
| Diameter of jets (mm) | 137.0 | 27.5 | 27.5 | 27.5 | 27.5 |
| Number of jets | 1 | 25 | 1 | 2 | 4 |
| Velocity of jet (m/s) | 5.0 | 5.0 | 5.0 | 5.0 | 5.0 |
| Initial pressure in vessel (MPa) | 0.17 | 0.17 | 0.17 | 0.17 | 0.17 |
| Volume above initial surface of water ($m^3$) | 50.0 | 50.0 | 50.0 | 50.0 | 50.0 |
| Initial temperature of pool of water (K) | 388.3 | 388.3 | 388.3 | 388.3 | 388.3 |
| Water subcooling (K) | 0.0 | 0.0 | 0.0 | 0.0 | 0.0 |
| Initial temperature of material in jet (K) | 3023.0 | 3023.0 | 3023.0 | 3023.0 | 3023.0 |
| Total mass flow rate of slumping material (kg/s) | 600.0 | 600.0 | 30.0 | 60.0 | 120.0 |
| Weight %age of $UO_2$ in slumping material | 66.7 | 66.7 | 66.7 | 66.7 | 66.7 |
| Weight %age of $ZrO_2$ in slumping material | 33.3 | 33.3 | 33.3 | 33.3 | 33.3 |
| Duration of slumping (s) | 10.0 | 10.0 | 10.0 | 10.0 | 10.0 |

In various cases, only diameter, and number of jets, and total mass flow rate of slumping material were varied. All other parameters were kept same for all the cases. A single large jet may slump onto the core plate, spreading the material in the jet over the plate and flowing through the holes in the core plate. The maximum mass flow rate of 600 kg/s is of the same order of magnitude as that in case of TMI-2 accident. SCDAP/RELAP5/MOD3.2 with the FCI model was used to calculate the behavior of the slumping material in all five cases and the results are shown in Table 4.

**Table 4.** Summary of results for FCI under conditions typical for severe accident in a PWR.

| Parameters as a result of FCI | Case 1 | Case 2 | Case 3 | Case 4 | Case 5 |
|---|---|---|---|---|---|
| Fraction of slumping material breaking-up | 0.17 | 0.26 | 1.0 | 1.0 | 1.0 |
| Mean diameter of particles (mm) | 0.50 | 0.50 | 0.50 | 0.50 | 0.50 |
| Pressure increase after 10 s of slumping (MPa) | 0.10 | 0.13 | 0.012 | 0.03 | 0.074 |
| Swell of water level (m) | 1.50 | 0.35 | 0.12 | 0.25 | 0.35 |

The fraction of the break-up material varied from 1.0 for the cases of a few small jets with

mass flow rates of 30 kg/s per jet to 0.17 for Case 1 of single large diameter jet with a mass flow rate of 600 kg/s. The pressure increase was a function of the number of jets. For the cases with small diameter jets (27.5 mm), the maximum pressure increase for the case of four jets was approximately six times greater than that for the corresponding case of a single jet. The calculated transient pressures for cases 1 and 2 with 600 kg/s slumping rate are compared in Figure 12. This figure shows that the slumping material falling through as several jets produces a more rapid rate of steam production and thus, a more rapid rate of pressure increase than the slumping material through as a single jet. Figure 12 also shows that for both cases pressure rise is significantly high during first 4 s of the slumping. The pressure rises for cases 3-5 are shown in Figure 13. For these three cases, the mass flow rate per jet was 30 kg/s and the number of jets varied from 1 to 4. The pressure increase for the four jet case is about six times than the pressure rise for the single jet case. The calculated values of transient liquid void fraction (1 – vapor void fraction) as a function of elevation are shown in Figures 14 and 15 for Case 1 and Case 2, respectively. If the initial water level was near the bottom of the reactor core, then then for both cases the swell in water level would have been sufficient to temporarily cover the bottom part of the core. If the bottom part of the core was embrittled, the temporary cover could result in cracking of the fuel rod cladding.

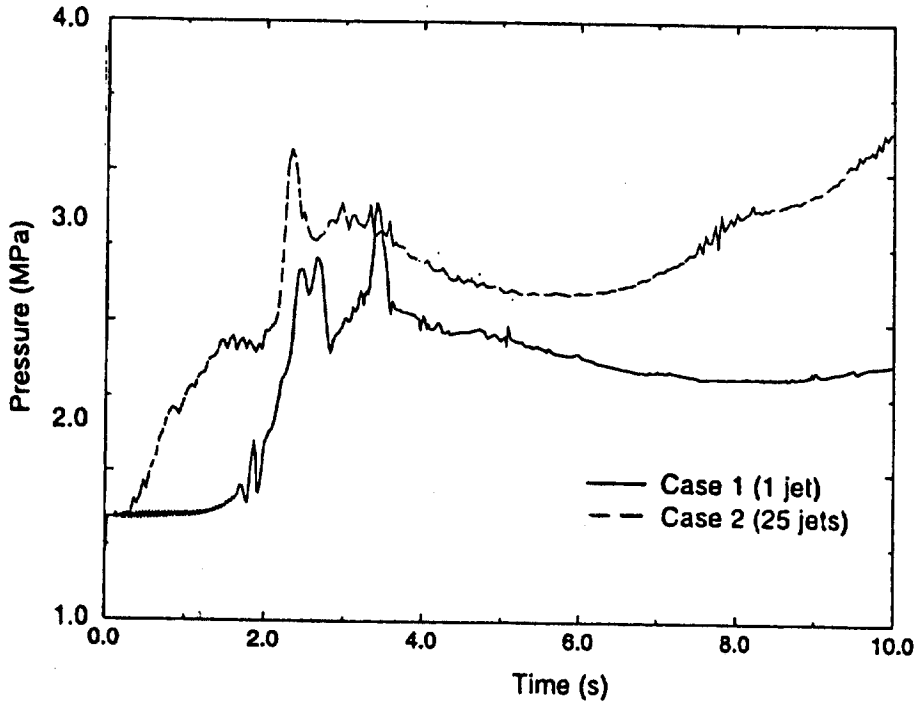


**Figure 12.** Calculated transient pressures in vessel for Case 1 (1 large jet) and Case 2 (25 small jets).

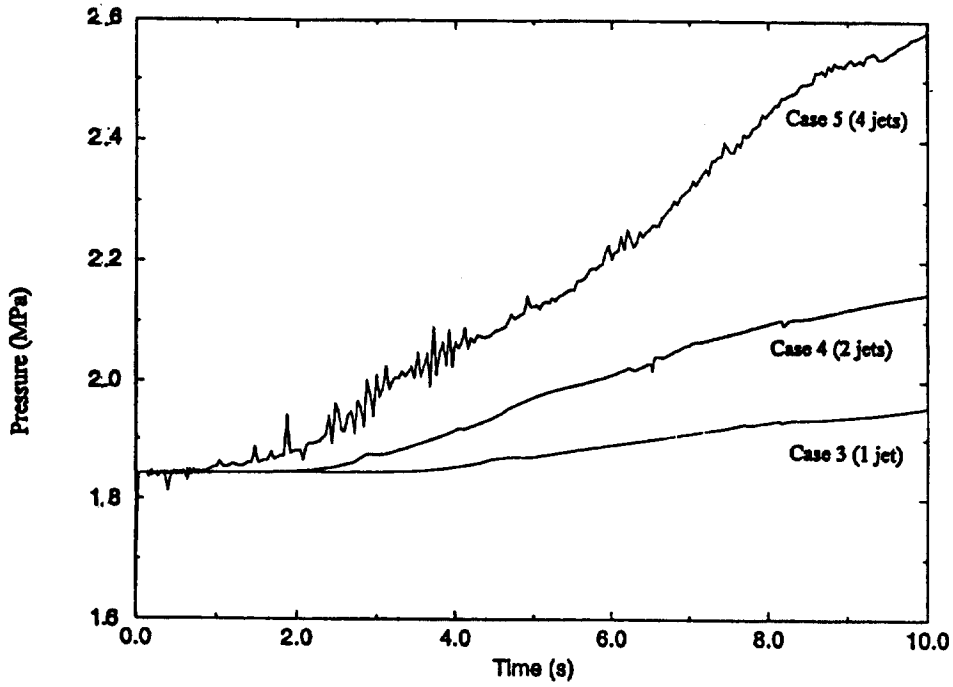


**Figure 13.** Calculated transient pressure in vessel for Case 2 (1 small jet), Case 4 (2 small jets), and Case 5 (4 small jets).

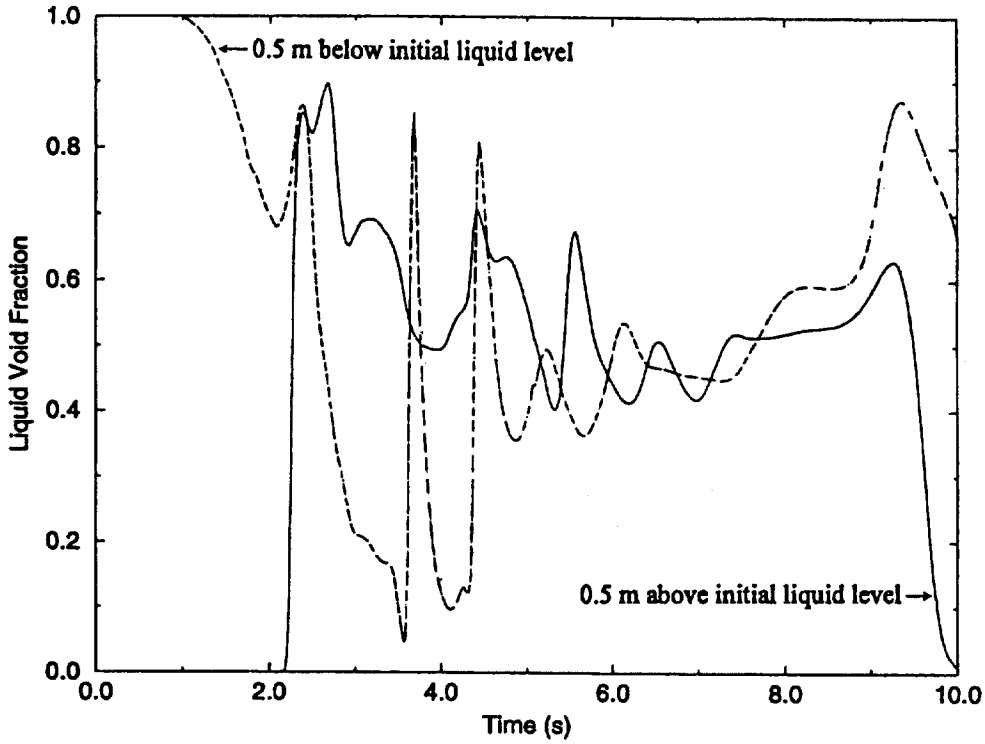


**Figure 14.** Transient liquid void fraction at various elevations for Case 1 (1 large jet).

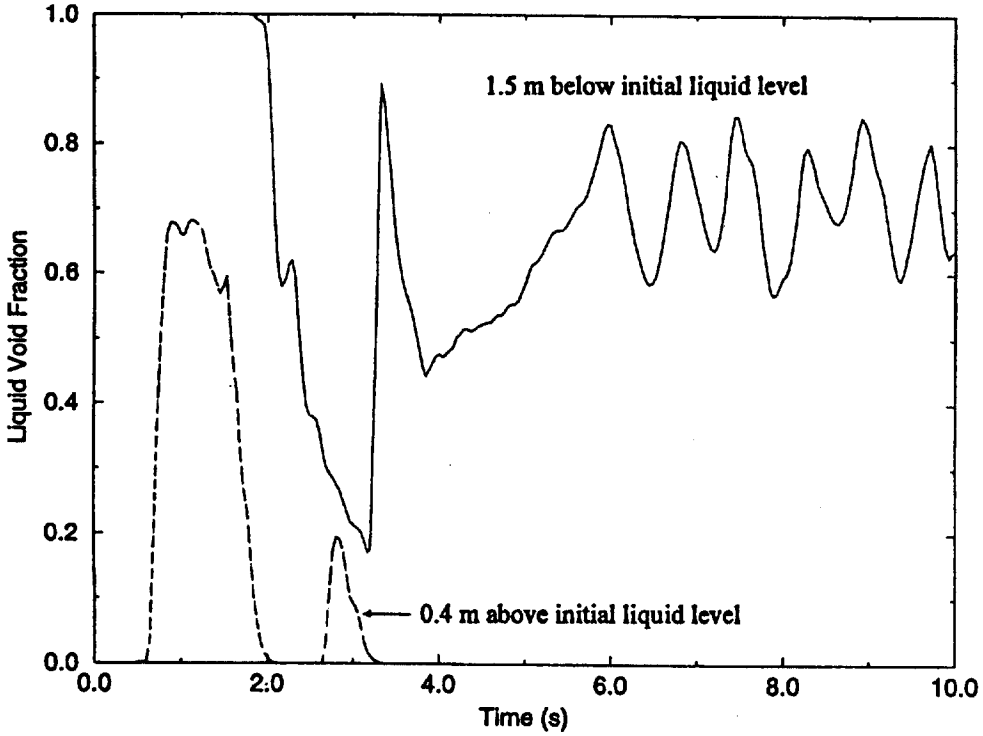


**Figure 15.** Transient liquid void fraction at various elevations for Case 2 (25 small jets).

### 4.3 Summary of Assessment Results

The limited assessment of the FCI model showed that the model is calculating several features of FCI fairly well. These features include the motion of the particles generated by FCI, the fraction of the slumping material, rate of steam production, and the maximum pressure increase as a result of FCI. If the slumping material divides into several jets, the break-up into particles is significantly more than that when the material slumps as a single jet. There are several areas of the model that can be improved if the need arises. Some of these are being heat transfer, material properties, size of the particles resulting from break-up, and vapor void fraction. The surface tension of a mixture of molten $UO_2$ and $ZrO_2$ with water needs to be accurately obtained. Flow regime prediction (by RELAP5) in the presence of FCI needs to be improved.

## 5. CONCLUSIONS

In this paper, we have described the phenomenon of nonenergetic molten fuel-coolant water interaction (FCI), various codes that model the FCI phenomenon, formation and break-up of fuel droplets, and associated thermal hydraulics. Verification and assessment of existing codes and models with experimental data were studied. Considering the requirements of SCDAP/RELAP5, the best option is to incorporate some one-dimensional FCI models from the code, TEXAS-V. A Lagrangian formulation of the fuel particles is used and is coupled with Eulerian formulation of RELAP5 thermal hydraulics. Experimental data obtained by Joint Research Center, Ispra, Italy (FARO series of tests) and at the University of California at Santa

Barbara (MAGICO-2000 series of experiments) were used to assess the FCI model. The assessment showed that the basic phenomena observed in the experiments are predicted reasonably by the present models. These phenomena being the motion of the particles generated by FCI, the fraction of the slumping material, rate of steam production, and the maximum pressure increase as a result of FCI. Various other assumptions used during the FCI analysis can affect the results, for example the fraction of the slumping material breaking-up, pressure rise. The modeling of FCI can be improved by: (1) more accurate correlation for the interfacial surface tension of molten $UO_2$ and $ZrO_2$ with water, and (2) more accurate definition of the flow regime in a region encountering FCI.

## 6. ACKNOWLEDGEMENTS

The authors would like to thank Prof. Michael Corradini of the University of Wisconsin, Madison, WI very useful and timely discussions regarding the TEXAS-V code. The U.S.-Nuclear Regulatory Commission program managers, late Dr. Yi Chen and Dr. Richard Lee provided useful guidance and support. Mr. Ed Harvego of the INEEL is being thanked for directing the entire effort. This work was performed under a contract DE-AC07-94ID13223.

## 7. NOMENCLATURE

$A$ = surface area

$A_p$, $A_{Li}$ = surface areas of the fuel droplet and the vapor-liquid interface, respectively.

$C_0$ = relates the cross-sectional area of the wavelet base ($8^2$) to the effective surface area (A) and is taken to be 0.01

$C_1$ = $0.1093-0.0785(\rho_c/\rho_p)^{0.5}$

$C_{fl}$ = boundary layer velocity profile factor, = $(4\nu_p/U_0)^{0.5}$

$C_{rad}$ = a constant representing the amount of radiation heat transfer from the fuel droplet absorbed in the continuous liquid,
= 1, if $T_L < T_{sat}$; = 0 to 1, if $T_L > T_{sat}$

$D_{BLS}$ = smallest stable droplet diameter

$D_p^n$, $D_p^{n+1}$ = fuel particle diameters at times $t^n$ and $t^{n+1}$, respectively

$D_{p,L}$ = drag between the particles and the surrounding liquid

$D_{p,g}$ = drag between the particles and the surrounding gas

$E_{p,k}$ = internal energy of the fuel particles

$E_p^n$ = internal energy of fuel particle at time $t^n$

$f_L$ = friction factor for flow of the particle through the liquid

$f_g$ = friction factor for flow of the particle through the vapor

$F_p$ = drag experience by the fuel particles while moving in the coolant

$F_{pL}$ = drag caused by the liquid

$F_{pg}$ = drag caused by the vapor

$F_{pi}$ = view factor between the fuel particle and the vapor-liquid interface

$$= \left[ 1 + \frac{(1-\varepsilon_p)}{\varepsilon_p} + \frac{A_p}{A_{Li}} \frac{(1-\varepsilon_p)}{\varepsilon_p} \right]^{-1}$$

$g$ = acceleration due to gravity

$h_{fg}$ = latent heat of evaporation

$h_{film}$ = convective film boiling heat transfer coefficient

$h_{free}$ = natural convection film boiling heat transfer coefficient

$h_{forced}$ = forced convection film boiling heat transfer coefficient

$h_{nc}$ = natural convection heat transfer coefficient averaged over a sphere (fuel droplet)

$h_{rad}$ = the radiation heat transfer between two concentric gray surfaces

$$= \sigma F_{pi} \frac{(T_p^4 - T_{sat}^4)}{\Delta T_{sat}}$$

$h_{sat}$ = saturated free convection film boiling heat transfer coefficient averaged over a sphere

$h_{tot}$ = total heat transfer from fuel droplets

$k_L$ = the thermal conductivity of liquid

$k_g$ = thermal conductivity of the vapor

$M_{KH}$ = mass of fuel broken-off from the jet because of K-H instability

$M_{p,k}$ = mass of fuel particles

$M_{BLS}$ = mass of fuel broken-off from the jet because of boundary layer stripping

$\dot{M}_{s,p}$ = steam generation rate when the fuel droplet is surrounded by a vapor film and continuous liquid

$n$ = time constant for disturbance waves

$n\lambda$ = growth speed of the disturbance wave with amplitude $\lambda$

$(n\lambda)_{max}$ = wavelength having the maximum growth rate

$q_p$ = volumetric internal heat generation rate in fuel material

$\dot{Q}_p$ = heat transfer from the fuel droplet to the surroundings

$\dot{Q}_{film}$ = convective (forced/free) film boiling heat transfer rat from the fuel particle to the vapor-liquid interface (between the vapor film and the continuous liquid) at the saturation temperature, $= \pi D_p^2 h_{film} (T_p - T_{sat})$

$\dot{Q}_{rad}$ = radiative heat transfer rate from the fuel droplet to the saturate vapor liquid interface (of the vapor film) at saturation temperature, $= \pi D_p^2 h_{rad} (T_p - T_{sat})$

$R$ = radius of the fuel jet

$Re$ = Reynolds number based on the relative velocity between the fuel droplet and surrounding liquid and fuel droplet diameter as the characteristic length,

$$= \rho_L D_p \frac{U_{rel}}{\mu_L}$$

$S_{p,k}$ = heat source (generated) term for the fuel particles

$t^n$, $t^{n+1}$ = time at steps n and n+1, respectively

$T_g$ = temperature of the gas surrounding the fuel particles
$T_L$ = temperature of the coolant liquid surrounding the fuel particles
$T_{p,k}$ = temperature of the fuel particles
$T_s$ = solidus temperature of fuel material
$T_{sat}$ = saturation temperature of water
$u_L$ = velocity of the liquid surrounding the fuel particles
$u_g$ = velocity of the gas surrounding the fuel particles
$u_{p,k}$ = velocity of the fuel particles
$U$ = melt velocity in the boundary layer thickness, $= U_0 / \exp[(R-r)/\delta]$
$U_0$ = melt velocity at the outer edge of the boundary layer in the moving frame
$U_{rel}$ = relative velocity between the fuel jet and the surrounding coolant
$We_{crit}$ = critical Weber number (may equal to 10-12)
$We$ = Weber number, $= \rho_c U_{rel}^2 D_p / \sigma_p$

**Greek Letters**

$\alpha_g$, $\alpha_L$ = void fractions of vapor and liquid phases, respectively
$\beta$ = coefficient of the thermal expansion of liquid
$\delta$ = melt velocity boundary layer thickness, $= 0.5\ C_{fl}\ (\pi R)^{0.5}$
$\delta_{film}$ = vapor film thickness (of the bubble) around the fuel droplet, $= \frac{h_{sat}}{k_g}$
$\Delta t_b$ = nondimensional time interval, $= U_{rel}\ (t^{n+1} - t^n)(\rho_c/\rho_p)^{0.5}/D_p^n$
$\Delta T_{sub}$ = liquid subcooling, $= (T_{sat} - T_L)$
$\Delta T_p$ = superheating of the fuel droplet, $= (T_p - T_{sat})$
$\varepsilon_p, \varepsilon_L$ = emissivities of the fuel particle and liquid, respectively
$\lambda$ = amplitude of the disturbance wave
$\mu_L$ = dynamic viscosity of the liquid (water)
$\nu_p$ = kinematic viscosity of the liquid fuel particles
$\rho_c$ = density of continuous fluid (water or steam)
$\Delta_L$, $\Delta_g$ = densities of liquid (water) and gas (steam), respectively
$\rho_p$ = density of molten fuel particles
$\sigma$ = Stefan Boltzman constant, $5.668 \times 10^{-8}$ W/(m$^2$·K$^4$)
$\Phi_L$ = surface tension of liquid (water)
$\sigma_p$ = surface tension of liquid fuel particles

## 8. REFERENCES

Abolfadl, M. A., Theofanous, T. G., 1987. An Assessment of Steam-Explosion-Induced Containment Failure, Part II: Premixing Limits. *Nuclear Science and Engineering*, **97**, pp. 282-295.

Allison, C. M., et al. SCDAP/RELAP5/MOD 3.2 Code Manual, Idaho National Engineering Laboratory, NUREG/CR-6150, November 1996.

Amarsooriya, W. H., Theofanous, T. G., 1991. Premixing of Steam Explosions: A Three Fluid Model. *Nuclear Engineering and Design*, **126**, pp. 23-39.

Angelini, S., Takara, E., Yuen, W., Theofanous, T. G., 1992. Multi phase Transients in the Premixing of Steam Explosions. In: *Proceedings of the Fifth International Meeting on Nuclear Reactor Thermal-Hydraulics (NURETH-5), Salt Lake City, UT, September 21-24,1992*, pp. 471-478.

Angelini, S., Yuen, W. W. Theofanous, T. G., 1995. Premixing-Related Behavior of Steam Explosions. *Nuclear Engineering and Design*, **155**, pp. 115-157.

Angelini, S., Theofanous, T. G., Yuen, W. W., 1995. The Mixing of Particle Clouds Plunging into Water. In: *Proceedings of the 7th International Meeting on Nuclear Reactor Thermal-Hydraulics (NURETH-7), Saratoga Springs, NY, September 10-15, 1995*, NUREG/CP-0142, pp. 1754-1778.

Bohl, W. R. An Investigation of Steam-Explosion Loadings with SIMMER-2, Los Alamos National Laboratory Report LA-10639-MS, March 1990.

Bromley, L. R., LeRoy, N. R., Robbers, J. A., 1953. Heat Transfer in Forced Convection Film Boiling, *Industrial and Engineering Chemistry, 45*, pp. 2639-2646.

Bürger, M., Cho, S. H., Berg, E. v., Schatz, A., 1995. Breakup of Melt Jets as Pre-Condition for Premixing: Modeling and Experimental Verification. *Nuclear Engineering and Design*, **155**, pp. 215-251.

Chandrasekhar, S. 1961. *Hydrodynamic and Hydromagnetic Stability*, Clarendon Press, Oxford, U. K., Chapters 10 and 11.

Corradini, M. L., 1991. Vapor Explosions: A Review of Experiments for Accident Analysis. *Nuclear Safety*, **32**, pp. 337-362.

Corradini, M. L., Kim, B. J., Oh, M. D., 1988. Vapor Explosions in Light Water Reactors: A Review of Theory and Modeling. *Progress in Nuclear Energy*, **22**, pp. 1-117.

Corradini, M. L., El-Beshbeeshy, M., Nilsuwankowsit, S., Tang, J., 1997. Fuel Fragmentation Model Advances Using TEXAS-V. In: *Proceedings of CSNI Specialists Meeting on Molten Fuel-Coolant Interaction, JAERI, Tokai-Mura, Japan.*

Chu, C. C., 1986. *One Dimensional Transient Fluid Model for Fuel-Coolant Interaction Analysis*, Ph. D. Thesis, University of Wisconsin, Madison, WI.

Chu, C. C., Corradini, M. L., 1989. One Dimensional Transient Fluid Model for Fuel/Coolant Interaction Analysis. *Nuclear Engineering and Design,* **101**, pp. 48-71.

Chu, C. C., Sienicki, J. J., Spencer, B. W. The THIRMAL-1 Computer Code for Analysis of Interaction Between a Stream of Molten Corium and a Water Pool, Electric Power Research Institute Report EPRI TR-103417, Volume 1 - Code Manual, Volume 2 – User's Manual, 1993.

Chu, C. C., Sienicki, J. J., Spencer, B. W., 1995. Validation of the THERMAL-1 Melt-Water Interaction Code. In: *Proceedings of the 7th International Meeting on Nuclear Reactor Thermal-Hydraulics (NURETH-7), Saratoga Springs, NY,* NUREG/CP-0142, pp. 2359-2389.

Denham, M. K., Tyler, A. P., Fletcher, D. F., 1992. Experiments on the Mixing of Molten Uranium Dioxide with Water and Initial Comparisons with CHYMES Code Calculations. In: *Proceedings of the Fifth International Meeting on Nuclear Reactor Thermal-Hydraulics (NURETH-5), Salt Lake City, UT,* pp. 1667-1675.

Dhir, V. K., Purohit, G. P., 1987. Subcooled Film-Boiling Heat Transfer from Spheres. *Nuclear Engineering and Design,* **47**, pp. 49-66.

Epstein, M., Fauske, H. K., 1985. Steam Film Instability and the Mixing of Core-Melt Jets and Water. In: *ANS Thermal Hydraulic Division Proceedings, ASME/AIChE National Heat Transfer Conference, Denver, CO,* pp. 277-284.

Fletcher, D. F., Denham, M. K., 1995. Validation of CHYMES Mixing Model. *Nuclear Engineering and Design,* **155**, pp. 85-96.

Fletcher, D. F., Thyagaraja, A., 1991. The CHYMES Coarse Mixing Model. *Progress in Nuclear Energy*, **26**, pp.31-61.

Fletcher, D. F., 1995, Propagation Investigations using the CULDESAC Model. *Nuclear Engineering and Design,* **155**, pp. 271-287.

Ginsburg, T., 1986. Liquid Jet Breakup Characterization with Application to Melt-Water Mixing. In: *Proceedings of the International ANS/ENS Topical Meeting on Thermal reactor Safety, San Diego, CA,* pp. 11.4-1—11.4-18.

Hall, R. W., Fletcher, D. F., 1995. Validation of CHYMES: Simulant Studies. *Nuclear Engineering and Design,* **155**, pp. 97-114.

Hohmann, H., Magallon, D., Schins, H., Yerkess, A., 1995. FCI Experiments in the Aluminum Oxide/Water System. *Nuclear Engineering and Design,* **155**, pp. 391-403.

Huhtiniemi, I., Hohmann, H., Magallon, D., 1995. FCI Experiments in the Corium/Water System. In: *Proceedings of the 7th International Meeting on Nuclear Reactor Thermal-Hydraulics (NURETH-7), Saratoga Springs, NY,* NUREG/CP-0142, pp. 1712-1727

Magallon, D., Hohmann, H., 1995. Experimental Investigation of 150-kg scale Corium Melt Jet Quenching in Water. In: *Proceedings of the 7th International Meeting on Nuclear Reactor Thermal-Hydraulics (NURETH-7), Saratoga Springs, NY,* NUREG/CP-0142, pp. 1688-1711.

Magallon, D., Hohmann, H., 1995. High Pressure Corium Melt Quenching Tests in FARO. *Nuclear Engineering and Design,* **155**, pp. 253-270.

Marshall, Jr., B. W., and Seebold, O. P. Reactor Safety Research Semi-annual Report, January-June 1985, Volume 33, Sandia National Laboratories, SAND85-1606, 1985.

Marshall, Jr., B. W., 1988. Recent Fuel-Coolant Interaction Experiments Conducted in the FITS Vessel. In: *ANS Thermal Hydraulic Division Proceedings, 25th ASME/AIChE National Heat Transfer Conference, Houston, TX,* pp. 265-275.

Medhekar, S., Amarasooriya, W. H., Theofanous, T. G., 1989. Integrated Analysis of Steam Explosions. In: *Proceedings of the Fourth International Topical Meeting on Nuclear Reactor Thermal-Hydraulics (NURETH-4), Karlsruhe, Germany,* **1**, pp. 319-326.

Mitchell, D. E., et al. *Intermediate Scale Steam Explosion Phenomena: Experiments and Analysis,* Sandia National Laboratories, SAND81-0124, NUREG/CR-2145, 1985.

Mitchell, D. E., Evans, N. A. *Steam Explosion Experiments at Intermediate Scale: FITB Series,* Sandia National Laboratories, SAND83-1057, 1986.

Nilsuwankosit, S., Moriyama, K., Corradini, M. L., 1996. Analysis of FARO-L14 Experiment with TEXAS. In: *ANS Thermal Hydraulics Division Proceedings, 31st National Heat Transfer Conference, Houston, TX,* pp. 16-26.

Rivard, W. C., Torrey, M. D. *K-FIX: A Computer Program for Transient, Two-Dimensional, Two-Fluid Model,* Los Alamos National Laboratory, LA-NUREG-6623, 1977.

Spencer, B. W., Wang, S. K., Blomquist, C. A., McUmber, L. M., Schneider, J. P. *Fragmentation and Quench Behavior of Corium Melt Streams in Water,* Argonne National Laboratory, Report ANL-93-32, NUREG/CR-6133, February 1994.

Theofanous,T. G., Saito, M., 1982. An Assessment of Class-9 (Core-Melt) Accidents for PWR Dry-Containment Systems. *Nuclear Engineering and Design,* **66**, pp. 307-332.

Theofanous, T. G., 1995. The Study of Steam Explosions in Nuclear Systems, *Nuclear*

*Engineering and Design,* **155**, pp. 1-26.

*Reactor Safety Study: An Assessment of Accident Risks in U. S. Commercial Nuclear Power Plant*, U. S. Nuclear Regulatory Commission, WASH-1400, NUREG-75/0114, 1975.

Young, M. F. *IFCI: An Integrated Code for Calculation of All Phases of Fuel-Coolant Interactions*, Sandia National Laboratories, SAND87-1048, NUREG/CR-5084, 1987.